Chemical Engineering Science 64 (2009) 4588–4596

Contents lists available at ScienceDirect

Chemical Engineering Science

journal homepage: www.elsevier.com/locate/ces

Extensional flow of wormlike micellar solutions

Michael Cromer[a,*], L. Pamela Cook[a], Gareth H. McKinley[b]

[a]Department of Mathematical Sciences, University of Delaware, Newark, DE 19716, USA
[b]Department of Mechanical Engineering, Massachusetts Institute of Technology, Cambridge, MA 02139, USA

ARTICLE INFO

Article history:
Received 27 September 2008
Received in revised form 31 March 2009
Accepted 1 April 2009
Available online 14 April 2009
Dedicated to Prof. M.M. Denn on the occasion of his 70th Birthday

Keywords:
Extensional flow
Viscoelasticity
Non-Newtonian fluids
Rheology
Constitutive modeling
Wormlike micelles

ABSTRACT

We consider the inhomogeneous extensional response of a new constitutive model, the VCM model [Vasquez, et al., 2007. A network scission model for wormlike micellar solutions I: model formulation and homogeneous flow predictions. J. Non-Newt. Fluid Mech. 144, 122–139] that has been developed to describe concentrated solutions of wormlike micelles. The time dependent numerical analysis is carried out in a simplified slender filament formulation appropriate for transient elongational flows of complex fluids. The simulations show that, beyond a critical extension rate, elongating filaments of a micellar fluid described by the VCM model exhibit a dramatic and sudden rupture event as a result of the scission of the entangled wormlike chains. The computations capture many of the features of the high-speed rupture process observed experimentally [Bhardwaj, et al., 2007. Filament stretching and capillary breakup extensional rheometry measurements of viscoelastic wormlike micelle solutions. J. Rheol. 51, 693–719] in filament stretching experiments with wormlike micelle solutions. The highly localized rupture predicted by the VCM model and the corresponding evolution in the tensile force within the filament is contrasted with the familiar and more gradual necking responses predicted by the upper convected Maxwell and Giesekus models under equivalent kinematic boundary conditions.

1. Introduction

Entangled solutions of wormlike micelles differ in a fundamental way from conventional polymer solutions because the entangled and reptating wormlike chains can break and reform, adding another independent relaxation mechanism to that of an entangled polymer network. This additional relaxation process can become highly localized under externally imposed shearing conditions leading to the formation of structures generically referred to as 'shear-bands'. The dynamics of these shear-banding events have been investigated extensively from both the experimental viewpoint (Hu and Lips, 2005; Miller and Rothstein, 2007; Boukany and Wang, 2008; Callaghan, 2008) and a theoretical context (Cates, 1987, 1996; Olmsted et al., 2000; Vasquez et al., 2007; Zhou et al., 2008b). Comprehensive recent reviews on the topic are provided by Cates and Fielding (2006), Fielding (2007) and Olmsted (2008).

The vast majority of these earlier investigations have focused on shearing flows in which the localization associated with microstructural disentanglement leads to a macroscopic kinematic domain or 'shear-band' over which the fluid rheology and the local velocity field vary rapidly. In the present paper we focus on strong extensional flows in which the macroscopic consequences of the local microstructural changes are less well documented, and harder to decipher because of the difficulty of isolating additional factors, such as surface tension, which affect the elastocapillary thinning of complex fluids such as entangled wormlike micelles. Rothstein (2008) recently reviewed what is known experimentally about extensional flows of these micellar systems. Early experiments by Yesilata et al. (2006) showed that the relaxation time of a micellar network inferred from capillary thinning experiments may be substantially different from that measured in shear. Bhardwaj et al. (2007) have shown experimentally, using an entangled system of 150/75 mM CPyCl/NaSal in brine (100 mM NaCl in distilled water), that the breakage event in filament stretching tests with wormlike micellar filaments can be quite different from that observed in other viscoelastic fluids. Instead of a smooth and global necking phenomenon, such as that seen in polymer solutions and melts (as well as in simulations with Newtonian fluids, and several viscoelastic constitutive equations such as the Giesekus model), the authors observed that beyond a critical strain a sudden and dramatic localized rupture took place in the micellar filaments. They attributed this behavior to a complete failure of the micellar network above a critical value of the local axial stress in the fluid column. A similar localized rupturing event was observed in filament stretching experiments with associative polymer solutions (Tripathi et al., 2006). The latter

* Corresponding author.
E-mail addresses: cromer@math.udel.edu (M. Cromer), cook@math.udel.edu (L.P. Cook), gareth@mit.edu (G.H. McKinley).

0009-2509/$ - see front matter © 2009 Elsevier Ltd. All rights reserved.
doi:10.1016/j.ces.2009.04.011

class of complex fluids also shows an elastic network connectivity that is very sensitive to the total stress placed on it. The constitutive model developed by Tripathi et al. (2006) for this telechelic network reflects this sensitivity by exhibiting a local maximum in the extensional viscosity at a finite extension rate. Although the majority of the constitutive models that have been proposed for describing wormlike micellar solutions have not been studied in strong extensional flows, it may be anticipated that if they show similar nonmonotonicity in the predicted constitutive response then they may also be able to capture the localized rupturing that has been observed during filament stretching experiments.

The specific constitutive model considered in this paper is the scission/reforming model developed in Vasquez et al. (2007). This model, derived from transient network theory, describes an entangled fluid in which long wormlike micelles, denoted species *A* (of length L), can break in half to form a second *B* species comprising two shorter (L/2) worms, which themselves can recombine to form one *A* chain. The model thus incorporates a highly simplified discrete version of the Cates (1987) 'living polymer' model for wormlike micelles. The breakage rate of the long entangled wormlike chains depends on the local stress and strain rate, and this leads to a coupling between the fluid microstructure and the global kinematics of the imposed flow. The model has been analyzed extensively in steady and transient inhomogeneous shearing flows (including steady shear, step strain and LAOS) by Zhou et al. (2008a, b) but the extensional rheology has not been considered to date.

In this article we investigate the response of the VCM model in filament stretching type experiments. In a filament stretching extensional rheometer (or 'FiSER') a small cylindrical fluid sample (of height L_0 and radius R_0) is constrained between two circular endplates which are then continuously separated at a prescribed rate. The evolution in the tensile force $F_z(t)$ exerted on the stationary endplate and the filament radius at the axial midplane $R_{mid}(t)$ are measured experimentally and used to evaluate the transient extensional viscosity of the fluid (see McKinley and Sridhar (2002) for details). In an ideal FiSER experiment, the plate separation is exponential in time, and we impose a displacement of the form $L(t) = L_0\, e^{\dot{\varepsilon}_0 t'}$ at the upper endplate, where $\dot{\varepsilon}_0$ is the (constant) elongation rate. If the sample is initially cylindrical and the role of the endplates constraining the sample is initially neglected, then the boundary conditions are consistent with a homogeneous uniaxial extensional flow. In dimensional coordinates the velocity field is $\mathbf{v}' = (v'_{r'}, v'_{\theta'}, v'_{z'}) = (-\dot{\varepsilon}_0 r'/2, 0, \dot{\varepsilon}_0 z')$ and the filament radius decreases uniformly in the axial direction as $r' = R_0\, e^{-(\dot{\varepsilon}_0 t'/2)}$. The effective strain experienced by the filament, $\varepsilon = \dot{\varepsilon}_0 t'$, is known as the Hencky strain.

The kinematics of this ideal experiment correspond to a homogeneous irrotational flow and direct integration of the constitutive relations describing the evolution of the stresses in the fluid leads to a steady state extensional viscosity, $\eta_E(\dot{\varepsilon}_0) = (\tau'_{zz} - \tau'_{rr})/\dot{\varepsilon}_0$, which depends only on the imposed strain rate. However, in an actual filament stretching experiment, the evolution in the stresses and the kinematics within the elongating fluid thread are coupled. The rigid confining endplates and the possibility of hydrodynamic instability in the flow lead to a spatially and temporally inhomogeneous flow in which the net tensile stress, $\sigma'_E = \tau'_{zz} - \tau'_{rr}$, depends on the local strain and strain rate. These flow inhomogeneities may decay or grow in time and can ultimately lead to filament breakup.

Our simulations with the VCM model are contrasted with those of other simple single species viscoelastic models which have been well studied under equivalent flow conditions such as the quasi-linear UCM (upper convected Maxwell) model and the nonlinear Giesekus model.

Recent analytical and numerical work on transient extensional flows of nonlinear viscoelastic models has concentrated especially on those fluids for which threads/jets break up due to elastic effects even in the absence of surface tension. Renardy (2000) has shown that in the absence of surface tension a fluid thread characterized by the Giesekus model will never break up in a strict mathematical sense when undergoing filament stretching; however, this asymptotic analysis shows that the radius of the thread decreases as an exponential of an exponential! From a pragmatic experimental point of view, the radius of the filament rapidly thins to submicron levels and for all practical purposes the elongating sample breaks in a smooth and slender manner. Hassager et al. (1998) examined the corresponding behavior of the Papanastasiou–Scriven–Macosko (PSM) model and showed numerically that, in contrast to the smooth but very rapid thinning predicted for the Giesekus model, the PSM model exhibited a failure in finite time. The simulations predicted an abrupt and almost 'instantaneous' decrease in the filament radius and corresponding tensile force which is coupled to elastic recoil at the ends of the elongating thread. Very recently Bhat et al. (2008) examined the coupled effects of elasticity and capillarity in filament stretching rheometry using the Giesekus, FENE-P and FENE-CR constitutive models. The computations reaffirmed earlier results of Yao et al. (1998) that the rate of necking in a Giesekus fluid is faster than that for a Newtonian fluid, despite the strain-hardening extensional response, and also showed that filament failure occurs increasingly rapidly as the effects of surface tension increase. As the magnitude of the elastic stresses was increased (by increasing the stretching rate and the Deborah number $De = \lambda\dot{\varepsilon}_0$) the strain to failure, $\varepsilon_f = \dot{\varepsilon}_0 t_f$ was found to decrease and ultimately reach a limiting value (Bhat et al., 2008). In this 'rapid stretching limit', relaxation processes in the necking fluid filament become negligible and the material response becomes dominated by the nonlinear elastic stresses (McKinley and Hassager, 1999). Filament failure can then be directly described by the Considère criterion and corresponds to the strain at which there is a local maximum in the tensile force in the filament (Malkin and Petrie, 1997). Malkin and Petrie (1997) also considered the case of sudden 'cohesive failure' in elongating filaments, which typically occurs above a critical stress corresponding to the cohesive strength of the material undergoing deformation. Cohesive failure is typically only observed in rubbers and entangled melts at tensile stresses of order MPa or higher, far larger than the values achieved in filament stretching of relatively low-viscosity fluids such as micellar fluids. We thus do not consider cohesive failure further in this work. Finally, we note that if viscous stresses dominate the material response at high deformation rates, then the material response close to breakup is not well described by the Considère criterion, as discussed elsewhere in this Special Issue (Petrie, 2009).

The marked difference between the response predicted by different viscoelastic constitutive models during rapid stretching at $De \gtrsim 0.25$ must be intimately connected to differences in the rheological material response predicted by the models in a simple homogeneous elongational flow. Renardy (2004) explored theoretically the sensitive connection between extensional rheology and dynamics of filament thinning by considering the capillary thinning of fluid jets using a generalized Phan-Thien–Tanner (GPTT) model. In this family of models, a numerical exponent a characterizes the highest order nonlinear term in the constitutive equation and can be systematically varied. For exponents in the range $a > 2$, a finite time elastocapillary breakup process was documented. More specifically, for values $2 < a \leqslant \frac{7}{3}$ the effects of surface tension impact (but do not drive) the elastic breakup process (because the capillary stresses are of comparable order to the elastic stresses in the thinning filament). For fluids with $\frac{7}{3} < a < 3$ self-similar solutions were found to exist that correspond to a purely elastic rupture process in which surface tension effects are unimportant. For the wormlike micellar constitutive model considered in the present work, the nonlinear terms result in a stress nonlinearity stronger than that in the original Giesekus or

PTT models (i.e. the highest order elastic stress terms correspond to $a > 2$). The quadratic stress terms are augmented in the VCM model by the rate- and stress-dependent scission of the long species. It may thus be anticipated that filament stretching simulations will show an elastically driven rupture process at high *De* even in the absence of surface tension.

This paper builds on numerous seminal contributions to rheology and non-Newtonian fluid dynamics that have been made by Denn et al. (1975). Free-surface simulations that incorporate the interactions of nonlinear fluid elasticity and capillarity were first performed by Bousfield et al. (1986). The filament stretching apparatus of specific interest in the present work was first simulated in detail by Shipman et al. (1991). To simplify the dynamics of the long thin filaments generated during the stretching process and incorporate the key role of the elastic tensile force in the elongating thread we utilize a general one-dimensional formulation of the same basic form pioneered by Matovich and Pearson (1969) for Newtonian and Coleman–Noll second order fluids and by Denn et al. (1975) for the upper-convected Maxwell fluid. For the constitutive model we utilize a recently developed transient network model of the same general class as those considered by Mewis and Denn (1983), with a nonlinear model parameter that must be determined either from a nonlinear shearing or from an extensional deformation. The importance of understanding extensional flows of complex fluids was highlighted by Denn (1990) in an early review. We also consider the linear stability of the resulting flow and its connection to the rheological predictions of the constitutive model in a manner similar to the work of Ho and Denn (1977). Finally, beyond a critical strain, the forces acting on the chains in the transient elastic network lead to a localized failure event that is broadly similar to the rupture beyond a critical stress studied by Joshi and Denn (2003). However, in contrast to the latter work, the availability of a full frame-invariant constitutive model for the entangled micellar fluid of interest allows us to follow the dynamical process of localized necking in the fluid filament.

2. Model/equations

As discussed above, the VCM model developed by Vasquez et al. (2007) is a two species model. The total number density of 'short' segments available is denoted n_T; and under equilibrium conditions some of these join to form a longer entangled species A (of length L). Thus $n_T = 2n_A + n_B$ where n_A, n_B are the local number densities of species A, B, respectively, at a particular position and time.

The (nondimensional) constitutive equations (Vasquez et al., 2007) are

$$De_A \frac{Dn_A}{Dt} = \frac{1}{2} c_{Beq} n_B^2 - c_A n_A \tag{1}$$

$$De_A \frac{Dn_B}{Dt} = -c_{Beq} n_B^2 + 2 c_A n_A \tag{2}$$

$$De_A \mathbf{A}_{(1)} + \mathbf{A} - n_A \mathbf{I} = c_{Beq} n_B \mathbf{B} - c_A \mathbf{A} \tag{3}$$

$$\in_B De_A \mathbf{B}_{(1)} + \mathbf{B} - \frac{n_B}{2} \mathbf{I} = \in_B [-2 c_B n_B \mathbf{B} + 2 c_A \mathbf{A}] \tag{4}$$

where $\mathbf{A}, \mathbf{B}$ are the second moments of the configuration distribution function for species A, B, respectively. Here the recombination rate c_{Beq} of the short unentangled chains is taken to be constant, whereas the breakage rate of the long entangled micelles depends on the strength of the flow as $c_A = c_{Aeq} + De_A(\xi/3)(\dot{\gamma} : (\mathbf{A}/n_A))$, where c_{Aeq} is the rate of micellar scission at equilibrium and $\dot{\gamma} = \nabla \mathbf{v} + \nabla \mathbf{v}^t$ is the rate of deformation tensor. The total stress in the entangled fluid is given by (in the absence of solvent)

$$\mathbf{\Pi} = p\mathbf{I} + (n_A + n_B)\mathbf{I} - \mathbf{A} - 2\mathbf{B}$$

These constitutive equations must be coupled to the equations of conservation of mass

$$\nabla \cdot \mathbf{v} = \mathbf{0} \tag{5}$$

and that of conservation of momentum

$$\nabla \cdot \mathbf{\Pi} = \mathbf{0} \tag{6}$$

where we assume that the fluid is sufficiently viscous that inertial effects are negligible throughout the flow.

Appropriate boundary conditions correspond to no-slip at the endplates, the kinematic condition for the free surface and a balance of normal and of tangential stresses at the free surface. In what follows we scale spatial coordinates by the initial dimensional radius R_0, time by $\dot{\varepsilon}_0^{-1}$ (where $\dot{\varepsilon}_0$ is the extension rate), velocity by $R_0\dot{\varepsilon}_0$ and stress by the plateau modulus G_0. For this paper we take the initial aspect ratio of the cylindrical sample in the filament stretching rheometer to be $L_0/R_0 = 1$. The relaxation of the A species is governed by a Deborah number $De_A = \lambda_A \dot{\varepsilon}_0$ and the parameter $\in_B = \lambda_B/\lambda_A$ is the ratio of the relaxation time of the short, B, worms to that of the longer, A, worms. The characteristic effective relaxation time of the network resulting from the combined effects of reptation and scission is $\lambda_{eff} = \lambda_A/(1 + c_{Aeq}\lambda_A)$. The effective Deborah number in a filament stretching test is thus $De = \lambda_{eff}\dot{\varepsilon}_0$. The effects of surface tension in a filament stretching test are commonly parameterized by an elastocapillary number $Ec = G_0 R_0/\sigma$. The model parameters used in the present work were selected from fitting the rheological properties of a 100 mM CPyCl/NaSal solution (in a 2:1 brine mixture) and are $c_{Aeq} = 0.9, c_{Beq} = 1.4$, $\in_B = 6 \times 10^{-4}$, $\xi = 0.3$, $\lambda_A/\lambda_{eff} = 1.9$, $Ec^{-1} = 0.3$, $n_T = 2 + \sqrt{2c_{Aeq}/c_{Beq}}$ (Vasquez et al., 2007; Pipe et al., 2008).

3. Viscometric (homogeneous) steady state predictions

We first consider the predictions of the VCM model in a viscometric (homogeneous in space and time) extensional flow. In uniaxial elongation, with the scalings given above, the velocity field is $\mathbf{v} = (v_r, v_\theta, v_z) = (-r/2, 0, z)$ and the corresponding locus of a Lagrangian label 'X' follows the equations $r_X = e^{-t/2}, z_X = e^t$. In biaxial extension (or uniaxial compression) the sign of the deformation rate changes so that $\mathbf{v} = (r/2, 0, -z)$ and $r_X = e^{t/2}, z_X = e^{-t}$. Since there is no spatial variation in the kinematics, the individual axial and radial components of the constitutive equations can be solved as coupled ODEs in time until the solutions reach a steady state. Alternatively the time derivative terms can be set to zero and the resulting set of coupled nonlinear algebraic equations solved.

The homogeneous steady state solution for the tensile stress σ_E as a function of *De* in uniaxial extension is shown in Fig. 1a and is contrasted with the corresponding solutions for the Giesekus ($\alpha = 1/2$) and UCM ($\alpha = 0$) models. It can be seen that the tensile stress σ_E increases monotonically with *De* for the UCM and Giesekus models whereas the dependence is nonmonotonic for the VCM model. The tensile stress σ_E in the VCM model first increases with *De* due to extension of the wormlike micelles but then abruptly decreases at higher *De* due to the stress-enhanced rate of micellar rupture. In Fig. 1b we show the model predictions expressed in terms of the steady uniaxial and biaxial extensional viscosities $\eta_E = \sigma_E/De$. In the inset we reproduce the experimental measurements of Walker et al. (1996) in an opposed jet apparatus also for a CPyCl/NaSal solution. Similar observations (in uniaxial extension only) have been reported for a TTaBr (tetradecyl trimethylammonium bromide)/NaSal wormlike micelle by Prud'homme and Warr (1994). Both the VCM model and the experimental results in uniaxial extension exhibit the expected Trouton viscosity, $\eta_E = 3\eta_0$, at low *De*, which then increases (extension thickening) before decreasing (extension thinning) at high *De*. By contrast, the predicted and measured biaxial viscosities show

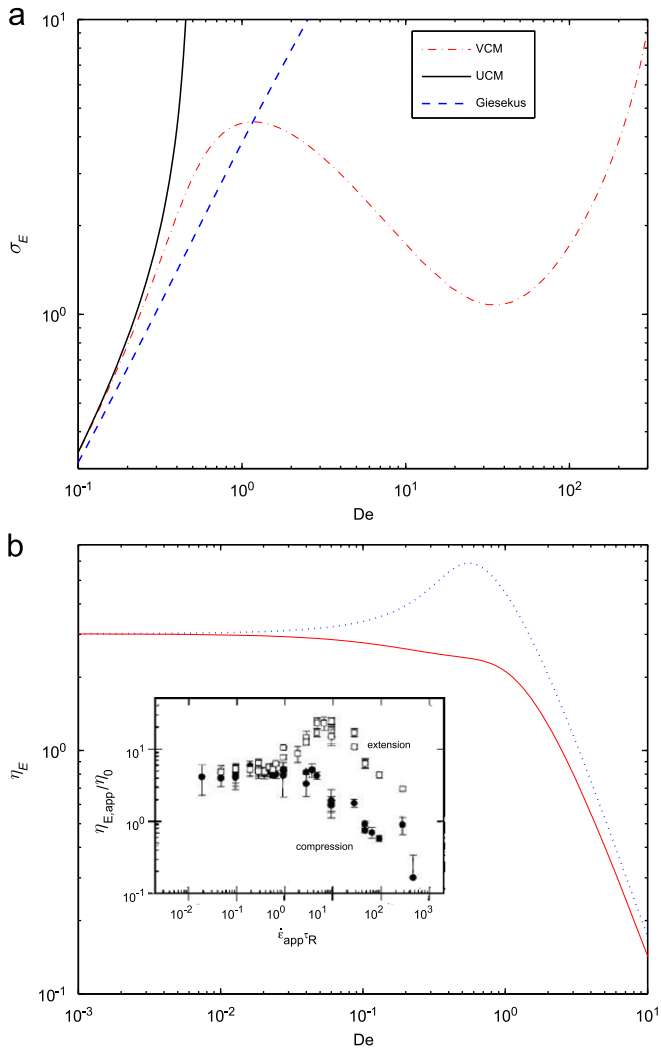

Fig. 1. Predictions of the VCM model in homogeneous steady-state extensional flow for the tensile stress as a function of extension rate: (a) the steady-state tensile stress $\sigma_E(De)$ in uniaxial extension compared to the UCM and Giesekus ($\alpha = \frac{1}{2}$) models, (b) predicted variation in the steady-state uniaxial extensional viscosity (blue, dash dot) and biaxial extensional viscosity (red, solid) compared with the experimental results of Walker et al. (1996) obtained with concentrated wormlike micellar solutions of CPyCl/NaSal in brine. (For interpretation of the references to color in this figure legend, the reader is referred to the web version of this article.)

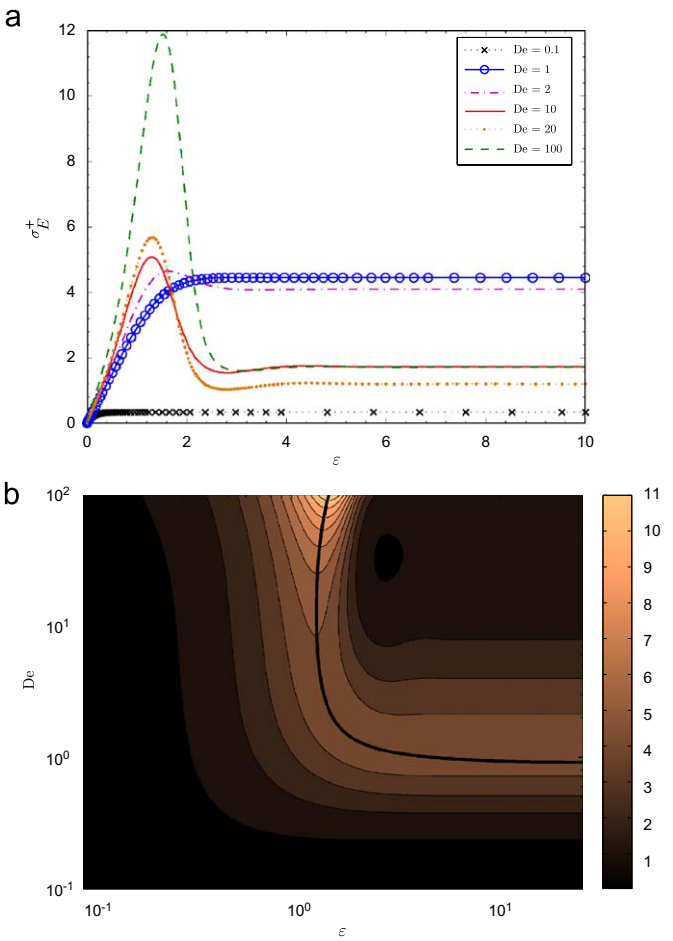

Fig. 2. Predictions of the VCM model in transient homogeneous uniaxial extension: (a) σ_E for several values of De as indicated; (b) contour plot showing the tensile stress $\sigma_E(De, \varepsilon)$ and the location of the maximal value $\sigma_{E,max}$ (thick line).

an initial plateau followed directly by a monotonic decrease (extension thinning) due to the kinematic differences of the biaxial extensional field.

In Fig. 2a we show the transient response of the homogeneous tensile stress growth function $\sigma_E^+(t)$ in start-up of steady elongational flow for several De. For small Deborah numbers the stress difference rises monotonically to its steady state value. However, as the Deborah number is increased further to $De = 2$, the tensile stress growth function $\sigma_E^+(t)$ overshoots its steady state, and eventually this is followed at higher De by an undershoot. As the Deborah number increases further, the magnitude of both the overshoot and the subsequent undershoot becomes more pronounced. By contrast, for the UCM and Giesekus models, the tensile stress in homogeneous flow always increases monotonically with the deformation rate. The variation in the tensile stress with both dimensionless time (or strain) $\dot{\varepsilon}_0 t'$ and dimensionless strain rate (or De) can be represented in the form of a contour plot as shown in Fig. 2b.

Transient experiments corresponding to the start-up of steady extensional flow correspond to horizontal trajectories across this surface at a constant value of De. For each Deborah number beyond a critical threshold $De \simeq 0.9$ there is a maximum in the tensile stress at a specific value of the strain. The location of this ridge in De, t (or De, ε) space can be well approximated for $De > 1$ by the expression $t_{max} = 1.25 + 2.5 \times 10^{-3} De + (0.35/(De - 0.9))$. This is shown by the thick line in the figure, which asymptotes to $De = 0.9$ for large strains.

Following Olagunju (1999), who examined the linear stability of transient uniaxial elongation of an Oldroyd-B fluid, we analyze the linear stability of this homogeneous elongational flow for the VCM fluid. Perturbations from the axially uniform base state within the one-dimensional, inertialess (thin filament) approximation were considered. Fig. 3 shows the fastest growing mode, ω_M, of the perturbation $v_z = z + \delta e^{\omega t} \sin(2n\pi(z e^{-t} - \frac{1}{2}))$ as a function of De for the VCM model. For $De \lesssim 0.25$ (corresponding approximately to the linear viscoelastic regime), the largest (real) eigenvalue is roughly constant and reduces to that of the UCM model, as reported in Olagunju (1999). Thus the flow is unstable (i.e. the elongating filament does not remain a perfect cylinder of exponentially decreasing radius, but in fact slowly necks); however, the perturbations grow slowly. As De increases, the UCM model predicts a progressive stabilization of the rate of filament thinning due to the exponential growth in the tensile stresses in the filament (Olagunju, 1999). By contrast, for the VCM model, there is a rapid increase in the growth rate of the instability for intermediate values of De where the homogeneous steady state

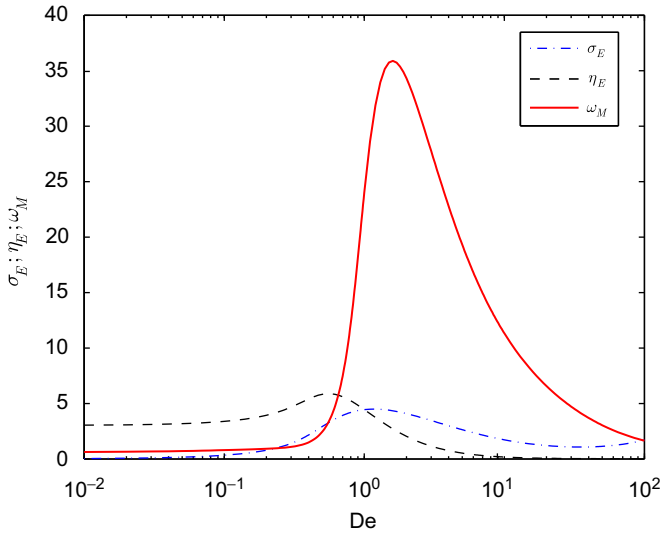

Fig. 3. Plot of the eigenvalue of the fastest growing mode, ω_M, of the perturbation to the transient homogeneous profile as a function of *De* for the VCM model (red solid line), along with the corresponding curves for σ_E and η_E. (For interpretation of the references to color in this figure legend, the reader is referred to the web version of this article.)

curve $\sigma_E(De)$ has multiple values of *De* for a given σ_E. At high Deborah numbers ($De > 2$) the growth rate of the instability decreases once more due to the increasingly important viscous contribution to the tensile stress difference arising from the short *B* species.

4. 1 + 1 Lagrangian model and predictions

In order to further investigate this instability in transient extensional flow and to capture the evolution of the axial inhomogeneities, we consider a slender filament approximation for the elongating fluid thread in a Lagrangian reference frame, analogous to the analysis of Renardy (1994). In this approximation, it is assumed that the dependent variables do not vary appreciably over any radial cross section of the long thin elongating filament; so that all properties depend on only the axial position, *z*, along the filament length and on the elapsed time (or total strain accumulated by each local material element).

In the Lagrangian formulation, following Renardy (1994, 2004), we denote the axial stretch by $s = (\partial z(X,t))/\partial X$ where *X* is the initial (reference) location of the particle and $z(X,t)$ is its current position. Conservation of mass then gives a relationship between the radius and the axial stretch $s = 1/r^2$. Conservation of linear momentum together with the free surface boundary conditions reduces (in dimensionless form) to

$$\frac{\sigma_E}{s} + \frac{Ec^{-1}}{\sqrt{s}} = f(t) \tag{7}$$

where the dimensionless force $f(t) = F_z(t)/(\pi G_0 R_0^2)$ must be determined as part of the solution. Physically, $f(t)$ is the total axial force in the filament which must be balanced by the tensile stresses carried at each axial location; namely the local axial stress multiplied by the local area plus the surface tension force multiplied by the local circumference. Since we are considering a slender filament approximation, the radial boundary condition can be used to replace the unknown pressure contribution to the total axial stress $T_{zz} = -p + \tau_{zz}$ by the radial extra stress τ_{rr}. The local strain rate at each axial slice is given by $u_{,z} = s_{,t}/s$. Smoothness of the solutions requires equivalence of the cross-derivatives, thus for consistency $s_{,t} = u_{,X}$. The evolution equation for the number density of long and short micellar chains becomes

$$De_A n_{A,t} = \frac{1}{2} c_{Beq} n_B^2 - c_{Aeq} n_A - \Xi \tag{8}$$

and

$$n_B = n_T - 2n_A \tag{9}$$

where $\Xi = (2\xi/3)\, De_A (s_{,t}/s)(A_{zz} - A_{rr})$ and n_T is the (fixed) total number of chain segments.

The individual components of the constitutive equations become

$$De_A \left(A_{zz,t} - 2\frac{s_{,t}}{s} A_{zz} \right) + A_{zz} - n_A = c_{Beq} n_B B_{zz} - c_{Aeq} A_{zz} - \Xi \frac{A_{zz}}{n_A} \tag{10}$$

$$De_A \left(A_{rr,t} + \frac{s_{,t}}{s} A_{rr} \right) + A_{rr} - n_A = c_{Beq} n_B B_{rr} - c_{Aeq} A_{rr} - \Xi \frac{A_{rr}}{n_A} \tag{11}$$

$$\epsilon_B De_A \left(B_{zz,t} - 2\frac{s_{,t}}{s} B_{zz} \right) + B_{zz} - \frac{n_B}{2} = -2\epsilon_B \left[c_{Beq} n_B B_{zz} - c_{Aeq} A_{zz} - \Xi \frac{A_{zz}}{n_A} \right] \tag{12}$$

$$\epsilon_B De_A \left(B_{rr,t} + \frac{s_{,t}}{s} B_{rr} \right) + B_{rr} - \frac{n_B}{2} = -2\epsilon_B \left[c_{Beq} n_B B_{rr} - c_{Aeq} A_{rr} - \Xi \frac{A_{rr}}{n_A} \right] \tag{13}$$

These constitutive relations, coupled to the momentum equation (7), represent coupled ordinary differential equations. The equation set is closed by recognizing that in a filament stretching rheometer (where we continuously pull the ends of the filament) the evolution in total sample length is given by

$$\int_0^1 s(X,t)\, dX = e^t \tag{14}$$

Finally, we note that in this one-dimensional slender filament approximation it is not possible to satisfy the no-slip boundary condition at the rigid endplates exactly (Yao et al., 1998; Olagunju, 1999) and consequently the radius of the filament at each end may increase or decrease slowly during the course of the simulation.

The initial profile is $s(X,0) = 1 - \delta\cos(2\pi X)$, $0 \leqslant X \leqslant 1$, and we choose the magnitude of the defect to be $\delta = 0.01$. For larger δ, the results are similar but occur at earlier times. All results presented are for $Ec^{-1} = 0$ since we are particularly interested in the possibility of elastic rupture/breakage due to micellar breakage in the absence of capillary effects. As discussed in the introduction, Renardy (2004) found that elongating filaments described by the upper convected Maxwell model or by the Giesekus model do not break in finite time in the absence of surface tension effects. Additional exploratory calculations (not presented here) using the VCM model with a finite value of the elastocapillary number (i.e. nonzero surface tension) show that capillarity does not change the mechanism of rupture, but rather only affects the time at which events occur.

5. Results

The solutions of Eqs. (8)–(14) were found using finite differences in time at each Lagrangian position *X* coupled with an iteration on the momentum equation to find *s* and *f* such that Eq. (14) is satisfied. The scheme used has optimal time steps of size 10^{-4} and spatial steps of size 10^{-2}; decreasing either step size did not affect the results except to give better resolution in figures. In order to compare and contrast the predictions of the VCM model with other familiar constitutive models (Giesekus, UCM), solutions for these models were also computed under the same conditions.

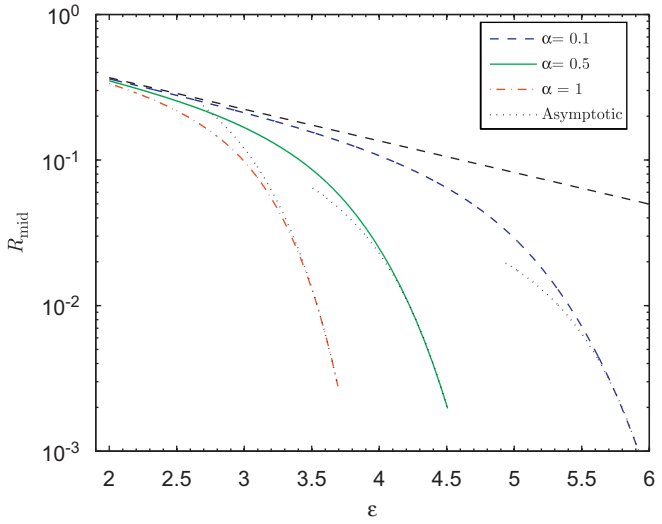

Fig. 4. Evolution of the axial midplane radius for the Giesekus model in the slender filament approximation at $De=2$ for $\alpha=0.1, 0.5, 1$ (respectively, dashed (blue), solid (green) and dash/dot (red) line). The results are plotted as a function of Hencky strain ε or nondimensional time and compared to Renardy's asymptotic solution near breakup (dotted lines). Parameters for the fits for Eq. (15) are: for $\alpha=0.1$; $c_0=0.07$, $c_1=1/61$; for $\alpha=0.5$; $c_0=0.17$, $c_1=1/15$; for $\alpha=1$; $c_0=0.65$, $c_1=1/4.5$. The upper dashed line shows the evolution in the midpoint radius for a homogeneous uniaxial extensional flow; $R=e^{-(t/2)}$. (For interpretation of the references to color in this figure legend, the reader is referred to the web version of this article.)

The theoretical analysis of Renardy (2000) found that the rate of radial thinning at the midaxial plane for the Giesekus model has the asymptotic form

$$R_{mid} = c_0\sqrt{\pi}c_1^{-(1/4)}\, e^{-(t/2)}\, e^{-((\alpha c_1/8\pi^2)\, e^{2t})} \tag{15}$$

where c_0, c_1 are constants of integration. Fig. 4 shows the agreement between the limiting behavior of the variation in R_{mid} computed for the Giesekus model and the asymptotic solution of Renardy for De=2, and for several values of the nonlinear constitutive parameter α in the Giesekus model. The filament radius clearly evolves smoothly toward zero at long times.

By contrast, simulations with the VCM model exhibit a much more rapid necking failure at a critical strain. The temporal evolution in the axial midplane radius $R_{mid}(t)$ (corresponding to a fixed Lagrangian label $X=0.5$) and in the tensile force $f(t)$ is shown in Fig. 5 for several different values of De. The radius of the neck initially follows ideal homogeneous uniaxial extension with $R_{mid} \sim e^{-(t/2)}$ (broken line). For small Deborah numbers, $De \lesssim 0.25$ (corresponding to the single valued portion of the steady state homogeneous flow curve), the radius continues to decrease smoothly in time, albeit at a rate that is slightly faster than the affine limit. This behavior is a reflection of the fact that the homogeneous solution is weakly unstable at all De (see Fig. 3). As De increases (to values that correspond to deformation rates for which the uniaxial homogeneous curve has multiple values of De for a given σ_E) the radius and the tensile force in the thread abruptly drop beyond a critical strain, denoted ε_f, corresponding to a finite-time rupture of the elongating filament. As De is further increased, the time at which this failure occurs decreases until it reaches a lower limiting value, and thereafter the time begins to slowly increase again at very high De. This can be seen quite clearly in a plot of the strain to failure (Fig. 6). The minimum strain to failure correlates well with the point of fastest instability growth rate shown in Fig. 3. The slow increase in ε_f at very high De corresponds to the weakly stabilizing effects of the viscous tensile stress originating from the short B species. There is a close connection be-

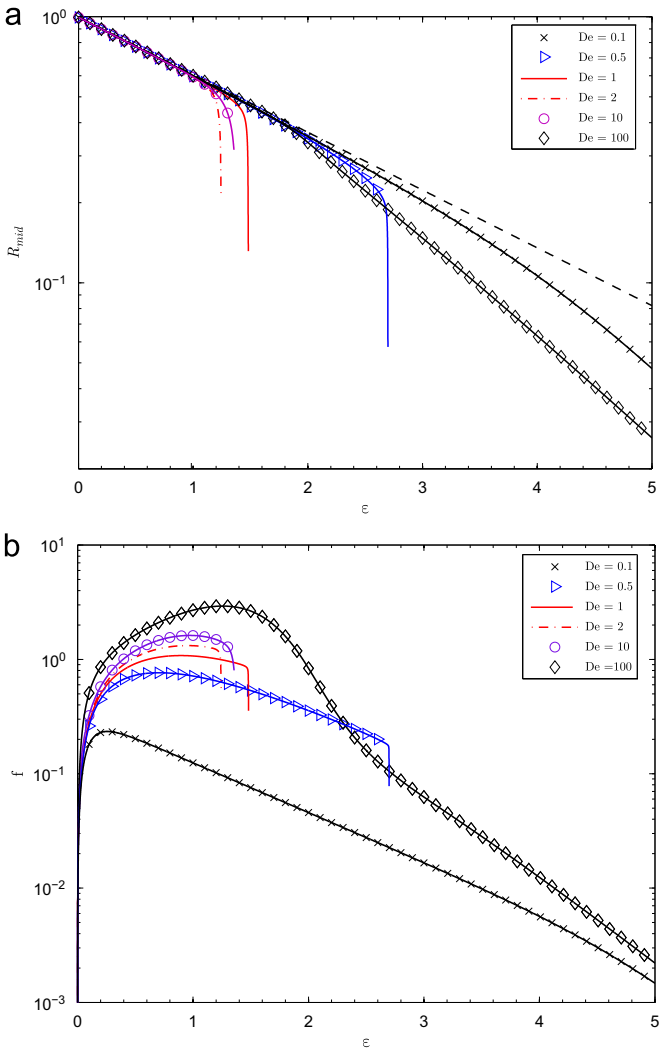

Fig. 5. Evolution in (a) axial midplane radius and (b) tensile force in an elongating filament as a function of Hencky strain for the VCM model at several De ($Ec^{-1}=0$).

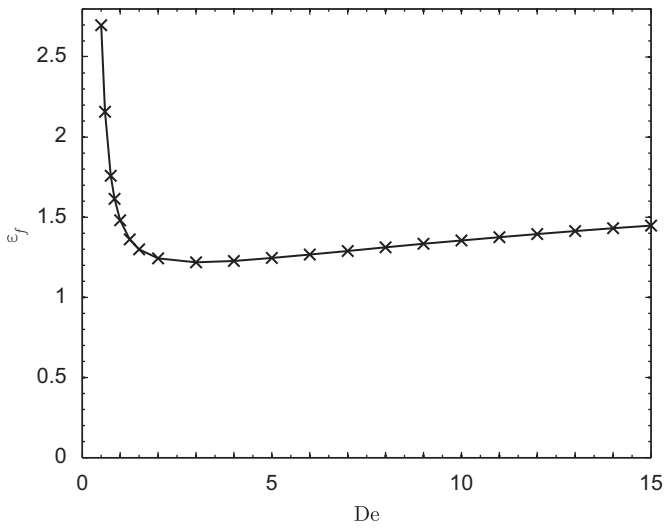

Fig. 6. Hencky strain at failure, ε_f, for the VCM model at each extension rate ($Ec^{-1}=0$).

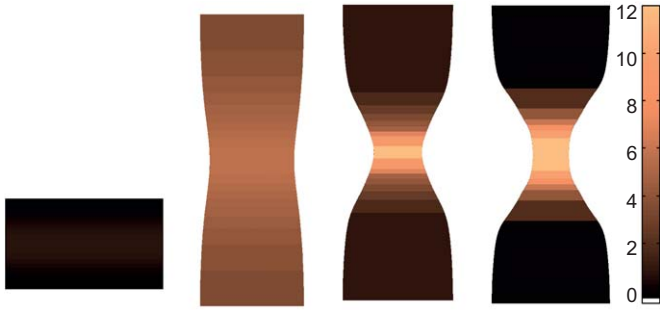

Fig. 7. Contour plots showing the evolution in the axial profile and the tensile stress $\sigma_E(z,t)$ in a VCM filament as a function of imposed Hencky strain. The scale is such that the darkest color indicates $\sigma_E = 0$, the lightest color that $\sigma_E = 12$. Note that the strain increments are not uniform, the strains at which the figures are shown correspond to 0.1, 1.2, 1.24 and 1.2433, the last being just before failure ($De = 2, Ec^{-1} = 0$).

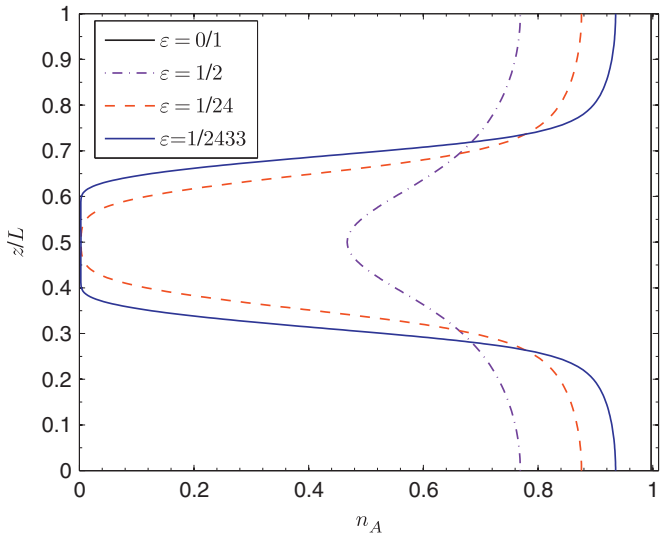

Fig. 8. $n_A(z)$ at the same Hencky strains as shown in Fig. 7 (ε=0.1, 1.2, 1.24, 1.2433) showing the spatial depletion (breakage) of species A in the highly thinned region under the extensional forcing (here $n_B = n_T - 2n_A$ where $n_T = 2 + \sqrt{2c_{Aeq}/c_{Beq}}$ (see Section 2)). Note that at $\varepsilon = 0.1$, $n_A \sim 1$, the right-hand boundary. In the region $0.4 \lesssim z/L \lesssim 0.6$, $n_A \sim O(10^{-3})$ for $\varepsilon = 1.2433$ ($De = 2, Ec^{-1} = 0$).

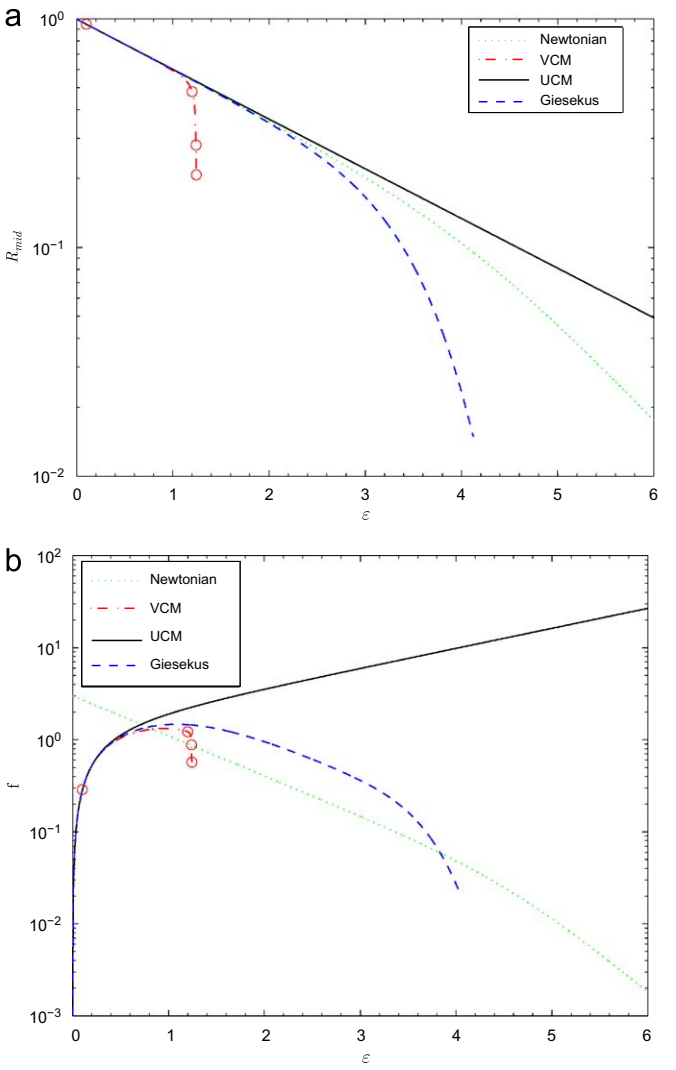

Fig. 9. Evolution in (a) the axial midplane radius and (b) the tensile force as functions of Hencky strain for the VCM, UCM and Giesekus ($\alpha = 1/2$) models at $De = 2$. Circles along the VCM curve in (a) and (b) correspond to the strains/times for which the filament is shown in Fig. 7. ($Ec^{-1} = 0$ and no solvent contribution).

tween the calculated strain to failure shown in Fig. 6 and the location of the ridge shown in Fig. 2b.

In Fig. 7 a sequence of snapshots shows the temporal evolution in the axial profile and the development of the tensile stress $\sigma_E(z,t)$ in the filament. During the initial stages of stretching, the deformation is close to ideal homogeneous extension; however, closer to the breakup time, the stress localizes and grows rapidly in the neck that begins to develop at the midaxial plane while relaxing to zero at the endplates. In Fig. 8 we show the evolution in the number density of the A species, n_A, along the filament for times corresponding to those in Fig. 7. Starting from a single equilibrium mixture of long, A, and short, B, chains (where $n_T = n_B + 2n_A$ is constant) the flow evolves, under large extensional forcing, into two spatially distinct phases. A comparison of the time evolution in $R_{mid}(t)$ for several different viscoelastic models at a fixed value of $De = 2$ is shown in Fig. 9a. The initial deviation from ideal uniaxial extension is similar for both the Giesekus and the VCM models; however, the deviation becomes far more drastic for the VCM model than for the Giesekus model. In Fig. 9b we show the corresponding evolution in the dimensionless tensile force $f(t)$ in the filament. The hollow circles correspond to the times at which the contour plots shown in Fig. 7 are presented. We emphasize that the trajectories for the VCM model are not truncated due to numerical resolution issues but because the one-dimensional slender filament formulation does not appear to admit a physical solution beyond this critical strain.

To further explore the dynamics of rupture at the midaxial plane we show in Fig. 10a the spatial variation in extension rate along the filament just before failure for the VCM model and for a Giesekus model. Although the evolution in the necking rate for the Giesekus model at the midplane is itself rapid, with $s \sim e^t e^{((c_1/16\pi^2)e^{2t})}$ so that $s_{,t}/s \sim O(e^{2t})$, for $\alpha = \frac{1}{2}$ (Renardy, 2000), the rupture is even more rapid and much more localized for the VCM model. In Fig. 10b we use the measure proposed by Bhat et al. (2008) to show the rate of viscoelastic energy storage/release along the filament for both models. In the VCM model the rate of work is negative close to the endplates corresponding to elastic unloading and recoil in the micellar fluid. This unloading is coupled to the extreme rate-dependent thinning in the extensional viscosity of fluid elements near the axial midplane and the rapid decrease in the tensile force in the filament.

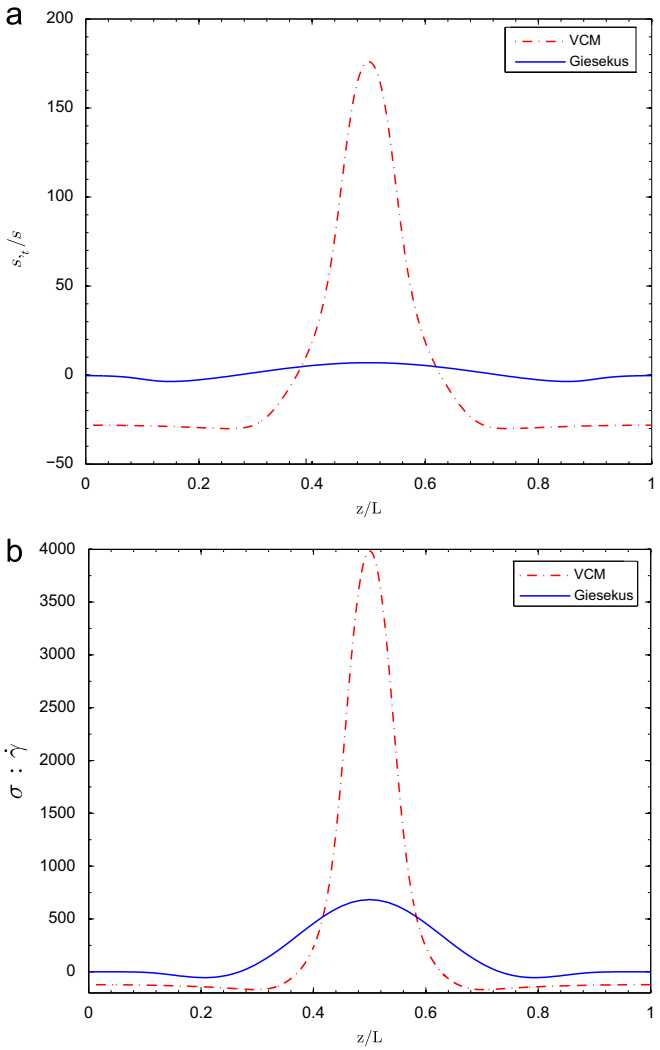

Fig. 10. (a) Comparison of the local extension rate in the filament as a function of scaled axial location $z/L(t)$ just before failure ($\varepsilon = 1.2433$ for the VCM filament, $\varepsilon = 4$ for the Giesekus filament ($\alpha = 1/2$) showing the sharply localized rate of thinning of the VCM filament close to rupture; (b) a measure of the energy storage or release rate showing the strongly enhanced elastic unloading (recoil) at the ends of the VCM filament as compared to the Giesekus filament ($Ec^{-1} = 0$).

6. Summary

In conclusion, we have considered the steady and transient elongational response of a nonlinear elastic network model developed for concentrated wormlike micellar solutions. In steady homogeneous flows the model appears to capture the differences in the rate-dependent uniaxial and biaxial extensional viscosities that has been measured in experiments. The model contains a single nonlinear constitutive parameter which controls the magnitude of the extensional thickening in the viscosity and which can, in principle, be determined by regression to corresponding experimental measurements. In the start-up of uniaxial elongation, the model predicts a maximum in the tensile stress difference at a critical strain due to the stress-enhanced rupture in the number of long entangled wormlike chains. The non-monotonic variation in the tensile stress resulting from a local increase in the deformation rate leads to the homogeneous uniaxial flow becoming increasingly unstable at moderate Deborah numbers. Transient simulations of the resulting inhomogeneous flow using a slender filament formulation show the formation of a localized neck in the filament at a finite Hencky strain. This necking event occurs even in the absence of capillarity and is a consequence solely of the nonlinear elastic response of the micellar network. This local elastic rupture event may be loosely considered the extensional analog of the well-documented shear bands that develop in steady and transient shearing flows of entangled micellar solutions (in which a non-monotonic variation in shear stress with shear rate results in the homogeneous flow becoming unstable and rapidly evolving to develop a spatially localized 'band' over which the rheological properties of the fluid rapidly vary). The general features of the VCM model predictions are consistent with the recent experimental observations of Bhardwaj et al. (2007), and result in a very rapid decrease in the filament radius near the midplane (see, e.g. Figs. 7 and 9a) at a value of the tensile force which is approximately constant (Fig. 5b) over a broad intermediate range of *De*. Future work will focus on quantitative comparison between experimental measurements and the VCM model, together with more detailed elucidation of the asymptotic behavior in the necking region—in order to understand how such rupture events can be directly connected to the precise functional form of the elongational viscosity of entangled fluids.

Acknowledgments

This research was supported by the NSF under DMS-0807395 and DMS-0807330.

References

Bhardwaj, A., Miller, E., Rothstein, J.P., 2007. Filament stretching and capillary breakup extensional rheometry measurements of viscoelastic wormlike micelle solutions. J. Rheol. 51, 693–719.
Bhat, P.P., Basaran, O.A., Pasquali, M., 2008. Dynamics of viscoelastic liquid filaments: low capillary number flows. J. Non-Newtonian Fluid Mech. 150, 211–225.
Boukany, P., Wang, S.Q., 2008. Use of particle-tracking velocimetry and flow birefringence to study nonlinear flow behavior of entangled wormlike micellar solution: from wall slip, bulk disentanglement to chain scission. Macromolecules 41, 1455–1464.
Bousfield, D.W., Keunings, R., Marrucci, G., Denn, M.M., 1986. Nonlinear analysis of the surface tension driven breakup of viscoelastic filaments. J. Non-Newtonian Fluid Mech. 21, 79–97.
Callaghan, P.T., 2008. Rheo NMR and shear banding. Rheol. Acta 47, 243–255.
Cates, M.E., 1987. Reptation of living polymers: dynamics of entangled polymers in the presence of reversible chain-scission reactions. Macromolecules 20, 2289–2296.
Cates, M.E., 1996. Flow behavior of entangled surfactant micelles. J. Phys. Condens. Mat. 8, 9167–9176.
Cates, M.E., Fielding, S.M., 2006. Rheology of giant micelles. Adv. Phys. 55, 799–879.
Denn, M., 1990. Issues in viscoelastic fluid mechanics. Annu. Rev. Fluid Mech. 22, 13–34.
Denn, M.M., Petrie, C.J.S., Avenas, P., 1975. Mechanics of steady spinning of a viscoelastic liquid. A.I.Ch.E.J. 21, 791–799.
Fielding, S.M., 2007. Complex dynamics of shear banded flows. Soft Mat. 2, 1262–1279.
Hassager, O., Kolte, M.I., Renardy, M., 1998. Failure and nonfailure of fluid filaments in extension. J. Non-Newtonian Fluid Mech. 76, 137–151.
Ho, T.C., Denn, M.M., 1977. Stability of plane Poiseuille flow of a highly elastic liquid. J. Non-Newtonian Fluid Mech. 3, 179–195.
Hu, Y.T., Lips, A., 2005. Kinetics and mechanism of shear banding in entangled micellar solutions. J. Rheol. 49, 1001–1027.
Joshi, Y.M., Denn, M.M., 2003. Rupture of entangled polymeric liquids in elongational flow. J. Rheol. 47, 291–298.
Malkin, A.Y., Petrie, C.J.S., 1997. Some conditions for rupture of polymeric liquids in extension. J. Rheol. 41, 1–25.
Matovich, M.A., Pearson, J.R.A., 1969. Spinning a molten threadline: steady-state isothermal viscous flows. I&ES Fund. 8, 512–520.
McKinley, G.H., Hassager, O., 1999. The Considère condition and rapid stretching of linear and branched polymer melts. J. Rheol. 43, 1195–1212.
McKinley, G.H., Sridhar, T., 2002. Filament stretching rheometry of complex fluids. Annu. Rev. Fluid Mech. 34, 375–415.
Mewis, J., Denn, M.M., 1983. Constitutive equations based on the transient network concept. J. Non-Newtonian Fluid Mech. 12, 69–83.
Miller, E., Rothstein, J.P., 2007. Transient evolution of shear banding in wormlike micelle solutions. J. Non-Newtonian Fluid Mech. 143, 22–37.
Olagunju, D.O., 1999. A 1-d theory for extensional deformation of a viscoelastic fluid under exponential stretching. J. Non-Newtonian Fluid Mech. 87, 27–46.
Olmsted, P.D., 2008. Perspectives on shear banding in complex fluids. Rheol. Acta 47, 283–300.

Olmsted, P.D., Radulescu, O., Lu, C.Y.D., 2000. Johnson–Segalman model with a diffusion term in cylindrical Couette flow. J. Rheol. 44, 257–275.
Petrie, C.J.S., 2009. Considère reconsidered: necking of polymeric liquids. Chem. Eng. Sci., doi:10.1016/j.ces.2009.03.004.
Pipe, C.J., Kim, N.J., McKinley, G.H., Vasquez, P.A., Cook, L.P., 2008. Wormlike micellar solutions II: comparison between experimental data and scission model predictions, in preparation.
Prud'homme, R.K., Warr, G.G., 1994. Elongational flow of solutions of rodlike micelles. Langmuir 10, 3419–3426.
Renardy, M., 1994. Some comments on the surface-tension driven break-up (or lack of it) of viscoelastic jets. J. Non-Newtonian Fluid Mech. 51, 97–107.
Renardy, M., 2000. Mathematical analysis of viscoelastic flows. In: CBMS-NSF Regional Conference Series in Applied Mathematics, SIAM 73.
Renardy, M., 2004. Self-similar breakup of non-Newtonian liquid jets. In: Binding, D.M., Walters, K. (Ed.), Rheology Reviews, vol. 2, pp. 171–196.
Rothstein, J.P., 2008. Strong flows of viscoelastic wormlike micelle solutions. In: Binding, D.M. Walters, K. (Ed.), Rheology Review. The British Society of Rheology, Aberystwyth, Wales, UK, to appear.
Shipman, R.W.G., Denn, M.M., Keunings, R., 1991. Mechanics of the falling-plate extensional rheometer. J. Non-Newtonian Fluid Mech. 40, 281–288.
Tripathi, A., Tam, K.C., McKinley, G.H., 2006. Rheology and dynamics of associative polymers in shear and extension: theory and experiments. Macromolecules 39, 1981–1999.
Vasquez, P.A., Cook, L.P., McKinley, G.H., 2007. A network scission model for wormlike micellar solutions I: model formulation and homogeneous flow predictions. J. Non-Newtonian Fluid Mech. 144, 122–139.
Walker, L.M., Moldenaers, P., Berret, J.F., 1996. Macroscopic response of wormlike micelles in elongational flow. Langmuir 12, 6309–6314.
Yao, M., McKinley, G.H., Debbaut, B., 1998. Extensional deformation, stress relaxation and necking failure of viscoelastic filaments. J. Non-Newtonian Fluid Mech. 79, 469–501.
Yesilata, B., Clasen, C., McKinley, G.H., 2006. Nonlinear shear and extensional flow dynamics of wormlike surfactant solutions. J. Non-Newtonian Fluid Mech. 133, 73–90.
Zhou, L., Ewoldt, R., Cook, L.P., McKinley, G.H., 2008a. Probing shear banding in entangled liquids using large amplitude oscillatory shear deformation. In: International Congress on Rheology, Monterey, CA, CF25.
Zhou, L., Vasquez, P.A., Cook, L.P., McKinley, G.H., 2008b. Modeling the inhomogeneous response and formation of shear bands in steady and transient flows of entangled liquids. J. Rheol. 52, 591–623.